Supporting Information

for

Effect of Imidazole and Phenolate Axial Ligands on the Electronic Structure and Reactivity of Oxoiron(IV) Porphyrin π-Cation Radical Complexes: Drastic Increase in Oxo-Transfer and Hydrogen Abstraction Reactivity

Akihiro Takahashi, Takuya Kurahashi, and Hiroshi Fujii*

Institute for Molecular Science and Okazaki Institute for Integrative Bioscience, National Institutes of Natural Sciences, and Department of Functional Molecular Science, The Graduate University for Advanced Studies, Myodaiji, Okazaki 444-8787 Japan

E-mail: hiro@ims.ac.jp

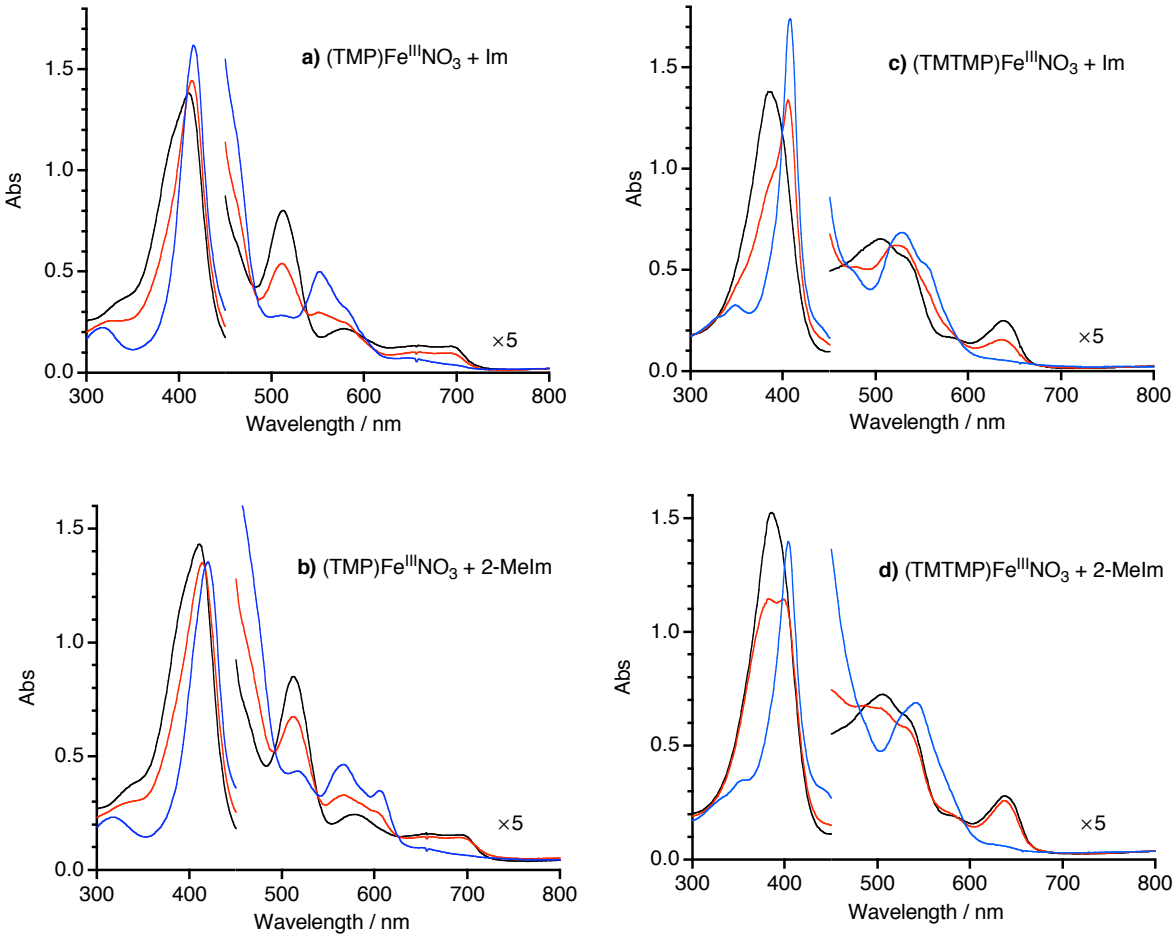

Figure S1. Absorption spectral changes for the titrations of (Por)Fe^{III}NO$_3$ with imidazole (Im) and 2-methylimidazole (2-MeIm) in dichloromethane at –80°C: **a)** (TMP)Fe^{III}NO$_3$ + Im; **b)** (TMP)Fe^{III}NO$_3$ + 2-MeIm; **c)** (TMTMP)Fe^{III}NO$_3$ + Im; **d)** (TMTMP)Fe^{III}NO$_3$ + 2-MeIm. Black lines; (Por)Fe^{III}NO$_3$, red lines; + 1.0 equiv of imidazoles, blue lines; + excess of imidazoles.

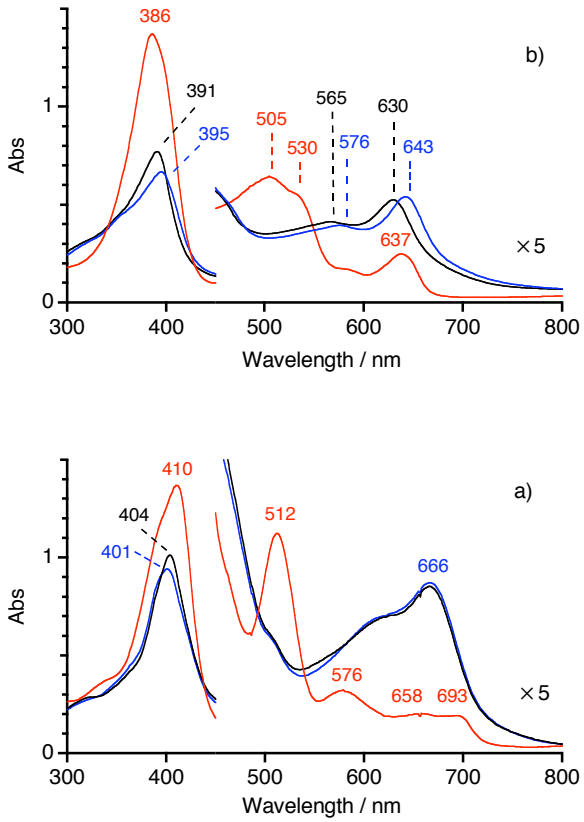

Figure S2. UV-visible absorption spectra of oxoiron(IV) porphyrin p-cation radical complexes (10 mM) with imidazole in dichloromethane at -80 °C. Red lines : $(P)Fe^{III}(NO_3)$, black lines : $(P^{+\bullet})Fe^{IV}O(NO_3)$, blue lines : $[(P^{+\bullet})Fe^{IV}O(Im)](NO_3)$. (a) P = TMP, (b) P = TMTMP.

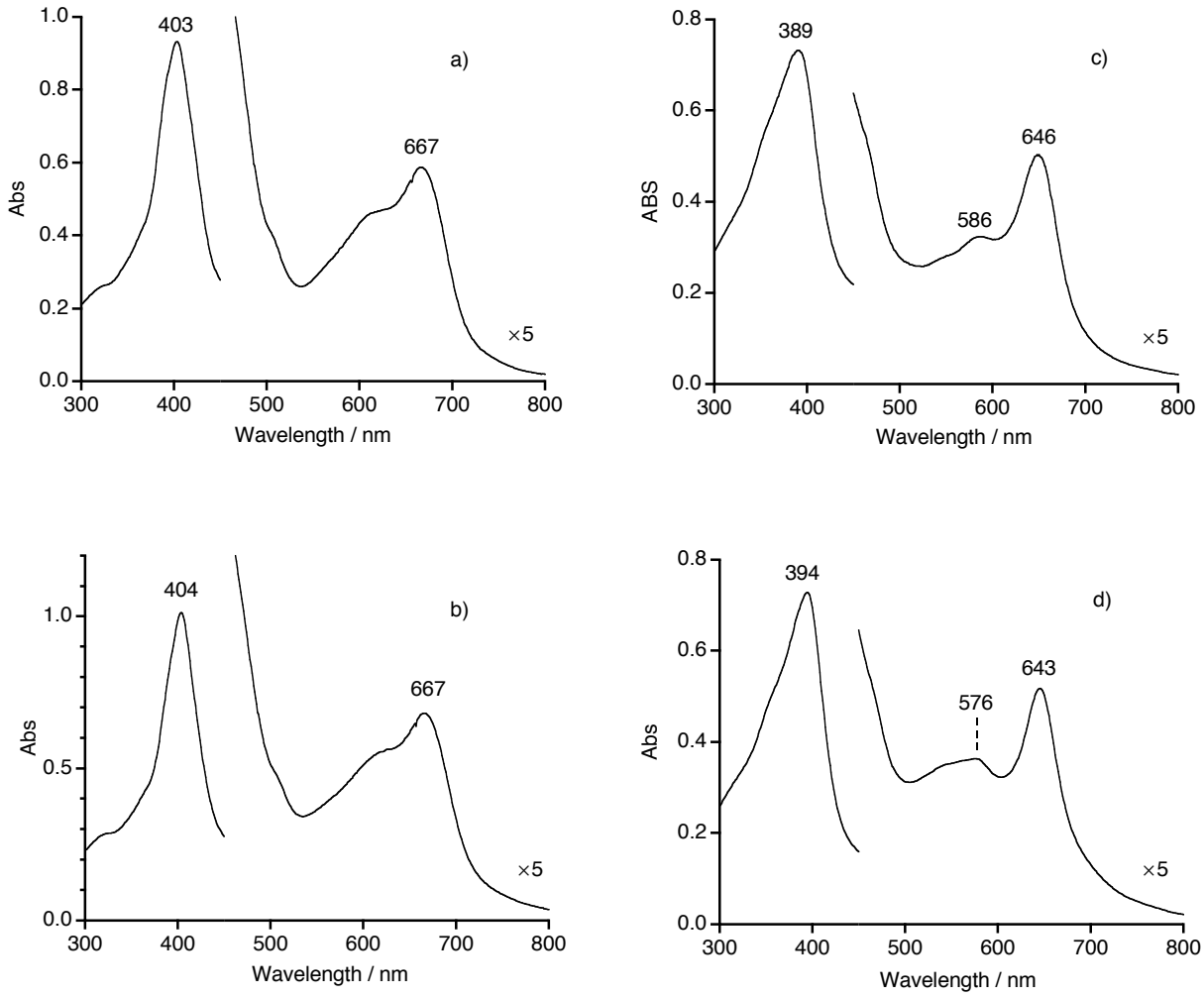

Figure S3. UV-vis absorption spectra of oxoiron(IV) porphyrin π-cation radical complexes (10μM) with 2-methylimidazole (2-MeIm) and 5-methylimidazole (5-MeIm) in dichloromethane at –80°C. a) $[(TMP^{+\bullet})Fe^{IV}O(2\text{-MeIm})](NO_3)$; b) $[(TMP^{+\bullet})Fe^{IV}O(5\text{-MeIm})](NO_3)$; c) $[(TMTMP^{+\bullet})Fe^{IV}O(2\text{-MeIm})](NO_3)$; d) $[(TMTMP^{+\bullet})Fe^{IV}O(5\text{-MeIm})](NO_3)$.

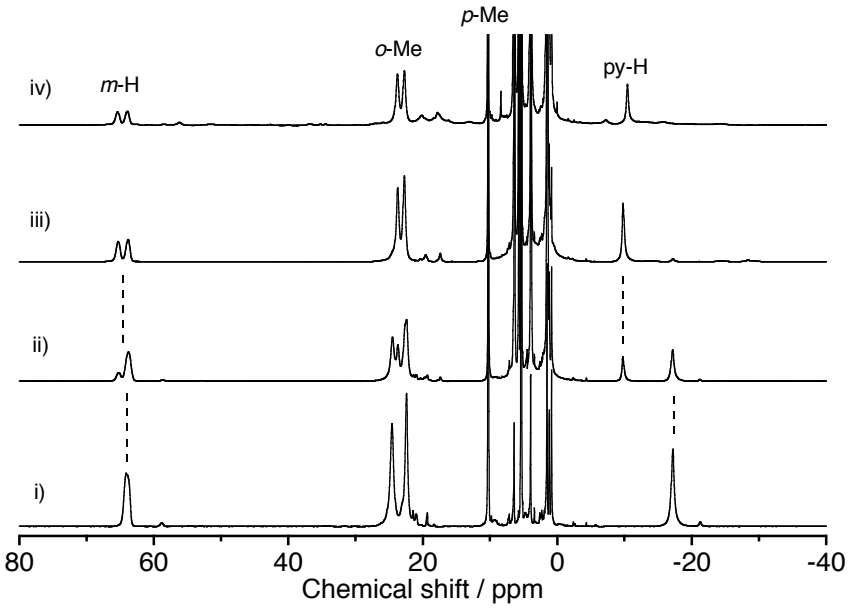

Figure S4. ^{1}H NMR spectral changes for the titration of $(TMP^{+\bullet})Fe^{IV}O(NO_3)$ with imidazole in dichloromethane-d_2 at –60°C: i) $(TMP^{+\bullet})Fe^{IV}O(NO_3)$; ii) i) + 0.4 equiv of Im; iii) i) + 1.1 equiv of Im; iv) $[(TMP^{+\bullet})Fe^{IV}O(Im)](ClO_4)$.

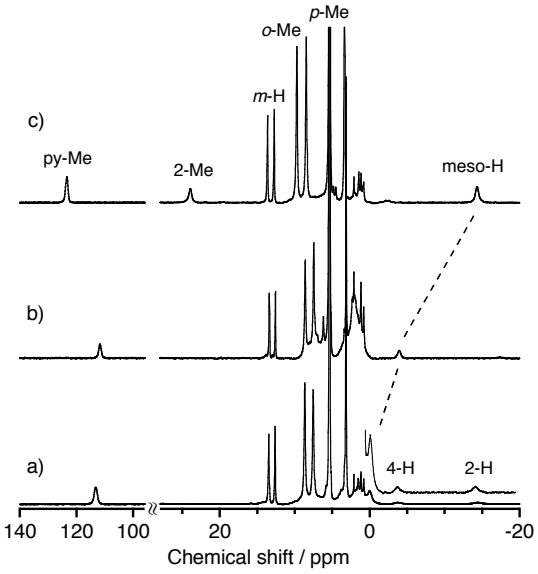

Figure S5. ^{1}H NMR spectra of $[(TMTMP^{+\bullet})Fe^{IV}O(L)](ClO_4)$ in dichloromethane-d_2 at –80 °C. a) L = Im, b) L = 5-MeIm, c) L = 2-MeIm.

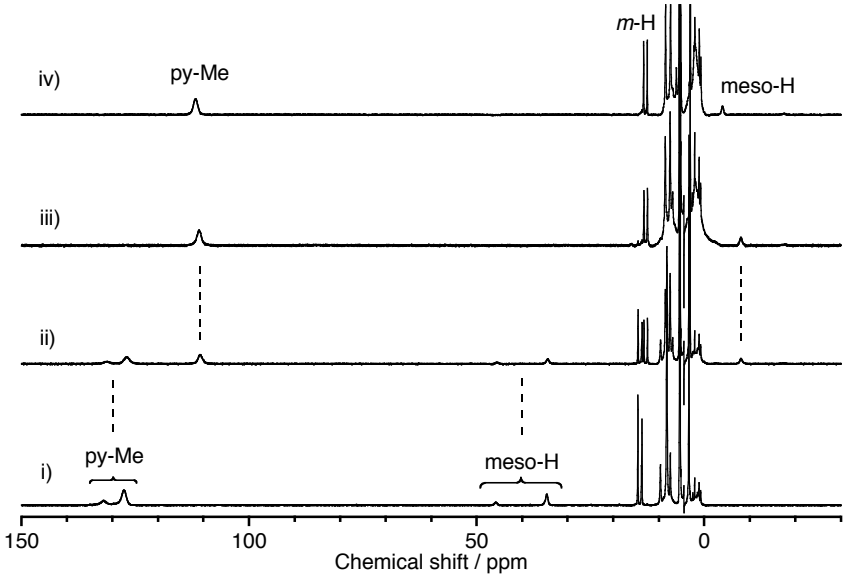

Figure S6. ^{1}H NMR spectral changes for the titration of (TMTMP$^{+\bullet}$)Fe^{IV}O(NO$_3$) with 5-methylimidazole in dichloromethane-d_2 at –80°C: **i)** (TMTMP$^{+\bullet}$)Fe^{IV}O(NO$_3$); **ii)** i) + 0.4 equiv of 5-MeIm; **iii)** i) + 1.1 equiv of 5-MeIm; **iv)** [(TMTMP$^{+\bullet}$)Fe^{IV}O(5-MeIm)](ClO$_4$).

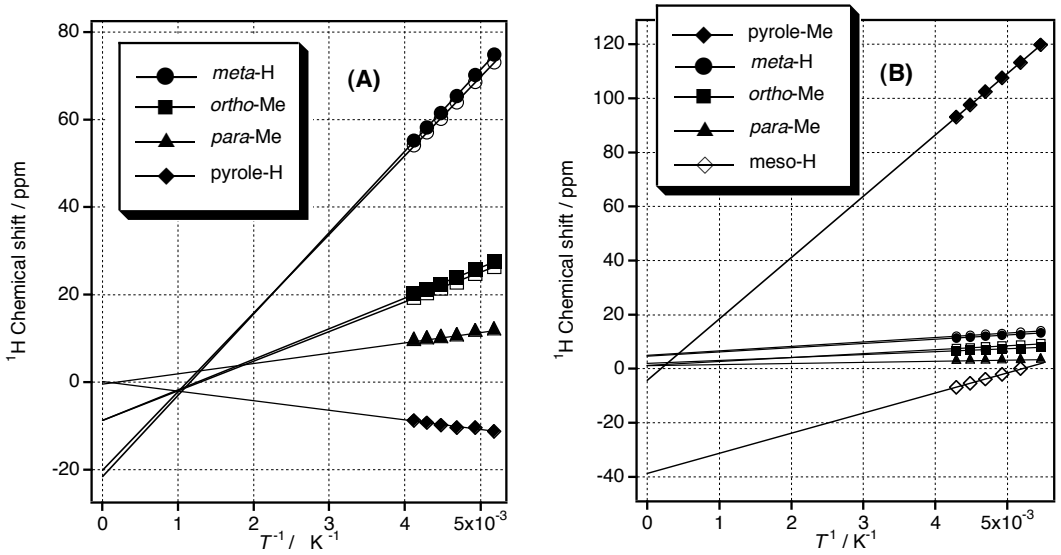

Figure S7. Curie plot of the ^{1}H chemical shifts versus reciprocal temperature. **(A)** [(TMP$^{+\bullet}$)Fe^{IV}O(Im)](ClO$_4$); **(B)** [(TMTMP$^{+\bullet}$) Fe^{IV}O(Im)](ClO$_4$).

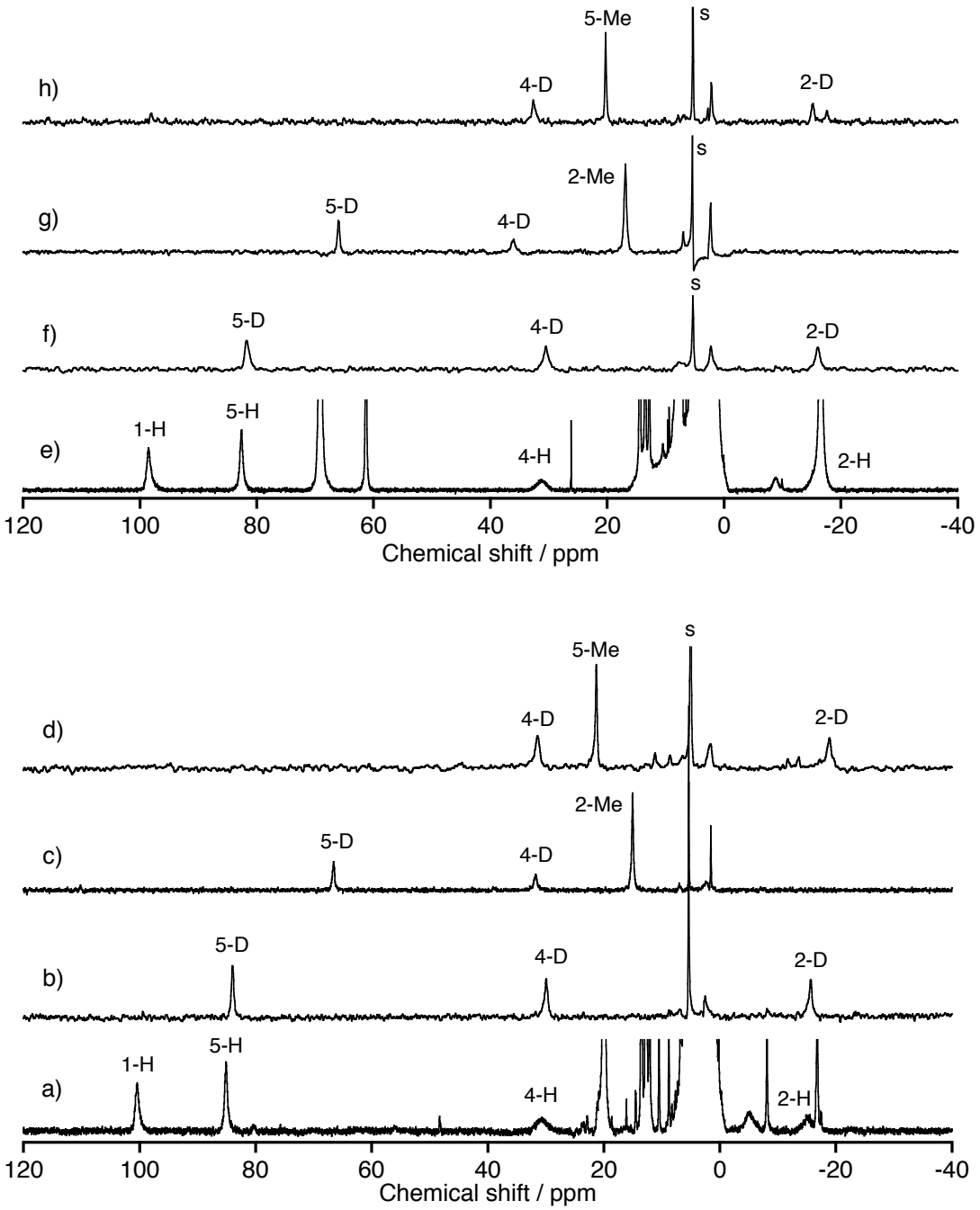

Figure S8. ^{1}H and ^{2}H NMR spectra of mono-Imidazole coordinated ferric porphyrin complexes in dichloromethane(-d_2) at 25°C: a) [(TMP)Fe^{III}(Im)](ClO_4); b) [(TMP)Fe^{III}(Im-d_4)](ClO_4); c) [(TMP)Fe^{III}(2-MeIm-d_6)](ClO_4); d) [(TMP)Fe^{III}(5-MeIm-d_6)](ClO_4); e) [(TMTMP)Fe^{III}(Im)](ClO_4); f) [(TMTMP)Fe^{III}(Im-d_4)](ClO_4); g) [(TMTMP)Fe^{III}(2-MeIm-d_6)](ClO_4); h) [(TMTMP)Fe^{III}(5-MeIm-d_6)] (ClO_4).

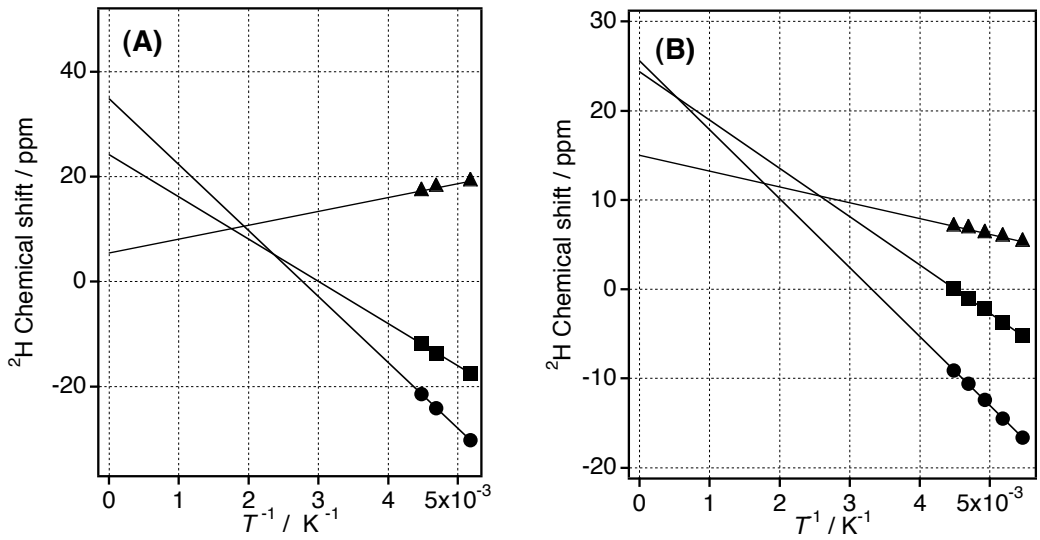

Figure S9. Curie plots for ^{2}H chemical shifts of the iron bound imidazole-d_4 (2-D;●, 4-D;■, 5-D;▲) of **(A)** [(TMP$^{+\bullet}$)Fe^{IV}O(Im-d_4)](ClO$_4$) and **(B)** [(TMTMP$^{+\bullet}$) Fe^{IV}O(Im-d_4)](ClO$_4$) versus reciprocal temperature.

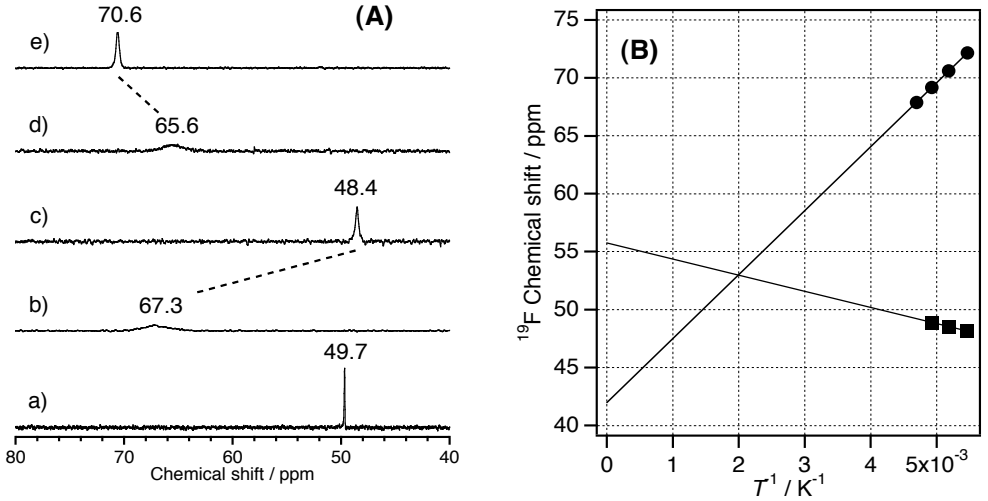

Figure S10. **(A)** ^{19}F NMR spectra of phenolate coordinated iron porphyrin complexes in dichloromethane-d_2 at –80°C: a) 3-fluoro4-nitrophenol; b) (TMP)Fe^{III}(3-F-4-NO$_2$-PhO); c) (TMP$^{+\bullet}$)Fe^{IV}O(3-F-4-NO$_2$-PhO); d) (TMTMP)Fe^{III}(3-F-4-NO$_2$-PhO); e) (TMTMP$^{+\bullet}$)Fe^{IV}O (3-F-4-NO$_2$-PhO). **(B)** Curie plot of the ^{19}F chemical shifts versus reciprocal temperature of the resonance: (TMTMP$^{+\bullet}$)Fe^{IV}O(3-F-4-NO$_2$-PhO); (●) and (TMP$^{+\bullet}$)Fe^{IV}O (3-F-4-NO$_2$-PhO); (■).

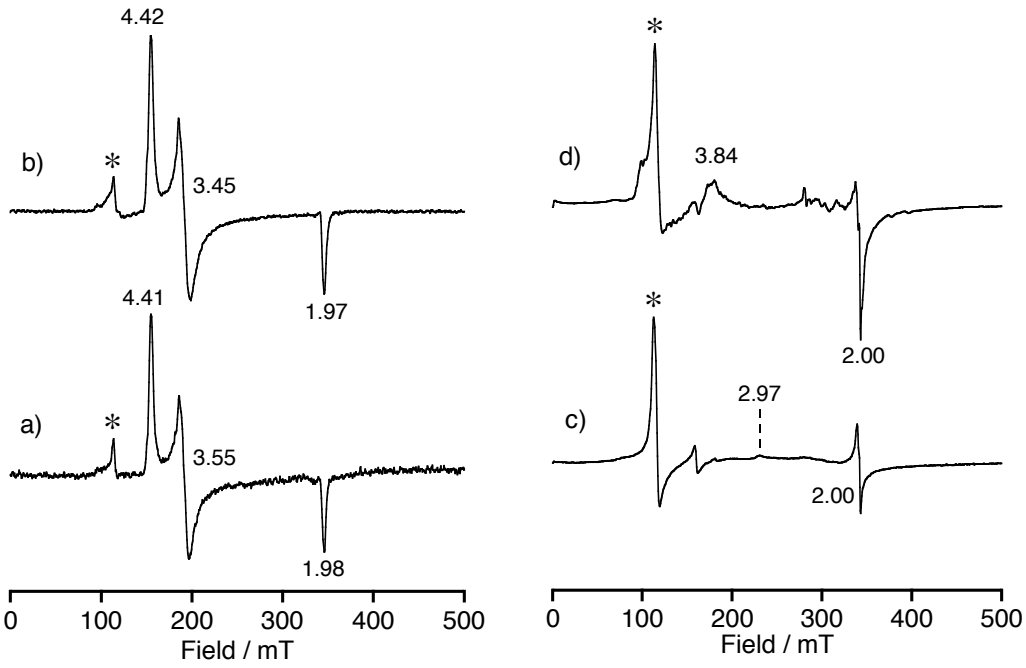

Figure S11. EPR spectra of imidazole coordinated oxoiron(IV) porphyrin π-cation radical complexes in dichloromethane-toluene (5:1) at 4K: a) $[(TMP^{+\bullet})Fe^{IV}O(Im)](ClO_4)$; b) $[(TMP^{+\bullet})Fe^{IV}O(5\text{-}MeIm)](ClO_4)$; c) $[(TMTMP^{+\bullet})Fe^{IV}O(Im)](ClO_4)$; d) $[(TMTMP^{+\bullet})Fe^{IV}O(5\text{-}MeIm)](ClO_4)$. Signals denoted by asterisks are due to unoxidized ferric mono-imidazole complex. These signal intensities indicated that the contents of these ferric complexes were less than 8 %. The EPR spectra of $[(TMP^{+\bullet})Fe^{IV}O(L)](NO_3)$ and $[(TMTMP^{+\bullet})Fe^{IV}O(L)](NO_3)$ were almost identical to those of $[(TMP^{+\bullet})Fe^{IV}O(L)](ClO_4)$ and $[(TMTMP^{+\bullet})Fe^{IV}O(L)](ClO_4)$, respectively.

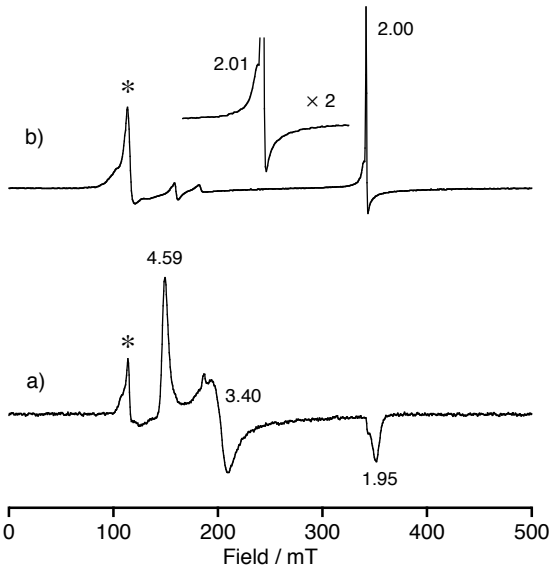

Figure S12. EPR spectra of a) $(TMP^{+\bullet})Fe^{IV}O$(3-F-4-NO_2-PhO) and b) $(TMTMP^{+\bullet})Fe^{IV}O$(3-F-4-$NO_2$-PhO) in dichloromethane-toluene (5:1) at 4 K. The signals denoted by asterisks exhibit signals for $(TMP)Fe^{III}$(3-F-4-NO_2-PhO) and $(TMTMP)Fe^{III}$(3-F-4-NO_2-PhO). Spin analyses of these peaks indicated that the contents of the unoxidized ferric complexes were less than 8 %. Presence of minor impurities of the unoxidized ferric complexes were confirmed by ^{1}H NMR spectra of $(TMP^{+\bullet})Fe^{IV}O$(3-F-4-NO_2-PhO) and $(TMTMP^{+\bullet})Fe^{IV}O$(3-F-4-$NO_2$-PhO), shown in Figure 4. Further oxidation of the sample solutions resulted in a decrease of the intensities of the EPR signals for $(TMP^{+\bullet})Fe^{IV}O$(3-F-4-NO_2-PhO) and $(TMTMP^{+\bullet})Fe^{IV}O$(3-F-4-$NO_2$-PhO).

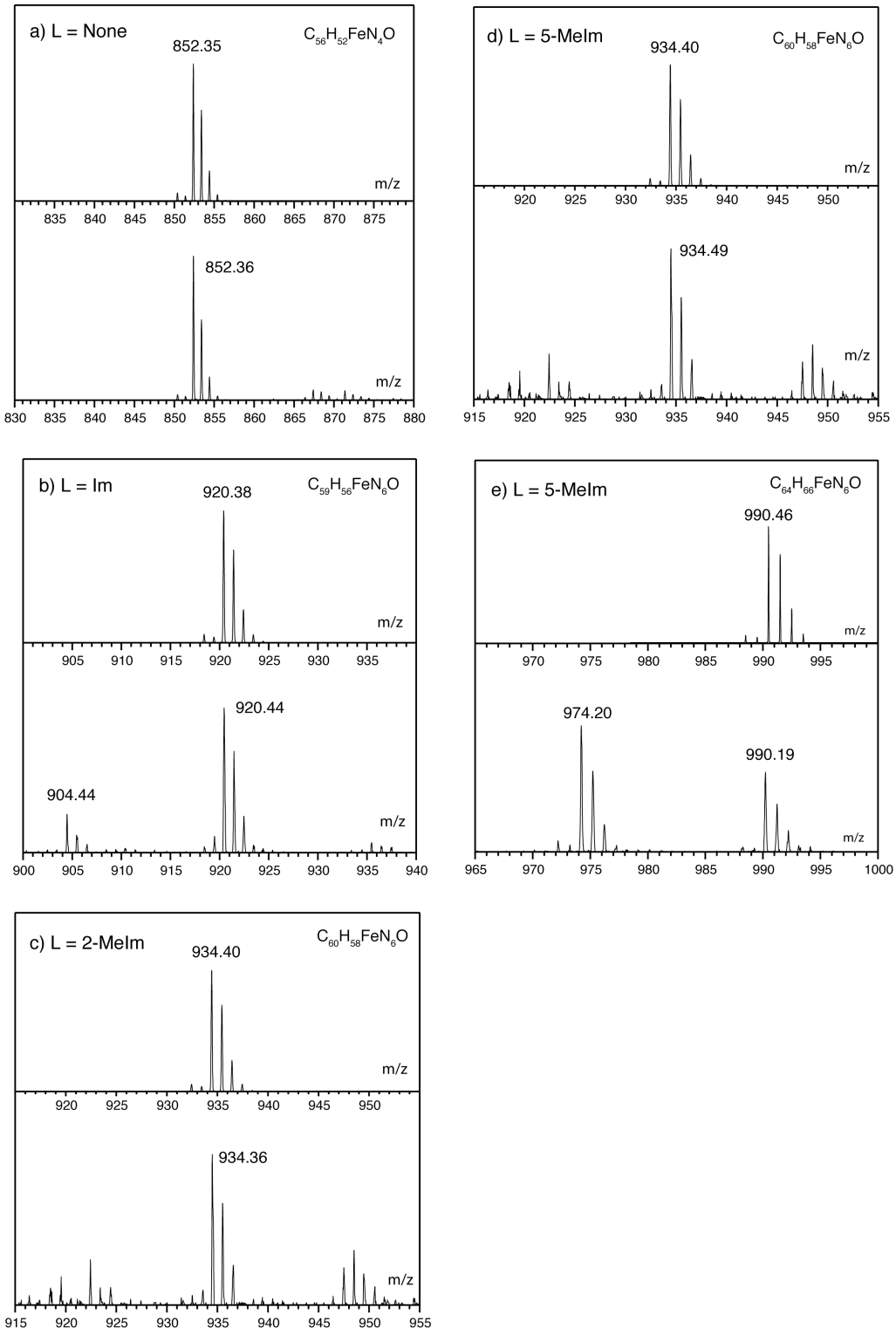

Figure S13. ESI-MS spectra of $[(TMP^{+\bullet})Fe^{IV}O(L)](ClO_4)$ (L = None, Im, 2-MeIm, 5-MeIm) taken in acetonitrile solution at low temperature: a) $[(TMP^{+\bullet})Fe^{IV}O](ClO_4)$; b) $[(TMP^{+\bullet})Fe^{IV}O(Im)](ClO_4)$; c) $[(TMP^{+\bullet})Fe^{IV}O(2\text{-}MeIm)](ClO_4)$; d) $[(TMP^{+\bullet})Fe^{IV}O(5\text{-}MeIm)](ClO_4)$; e) $[(TMTMP^{+\bullet})Fe^{IV}O(5\text{-}MeIm)](ClO_4)$. Observed (bottom) and calculated (top) isotope distribution patterns.

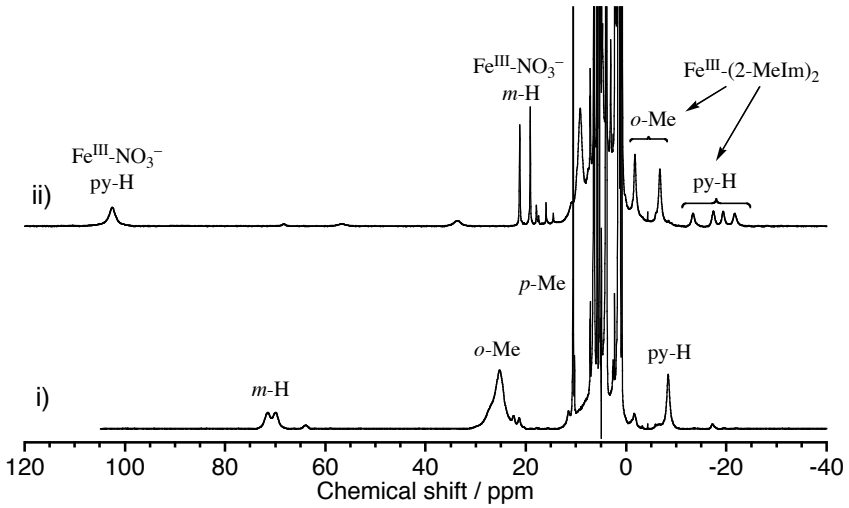

Figure S14. ^{1}H NMR spectral changes for the reaction of [(TMP$^{+\bullet}$)Fe^{IV}O(2-MeIm)](NO$_3$) with cyclooctene in dichloromethane-d_2 at –60°C: **i)** [(TMP$^{+\bullet}$)Fe^{IV}O(2-MeIm)](NO$_3$); **ii)** i) + 10 equiv of cyclooctene.

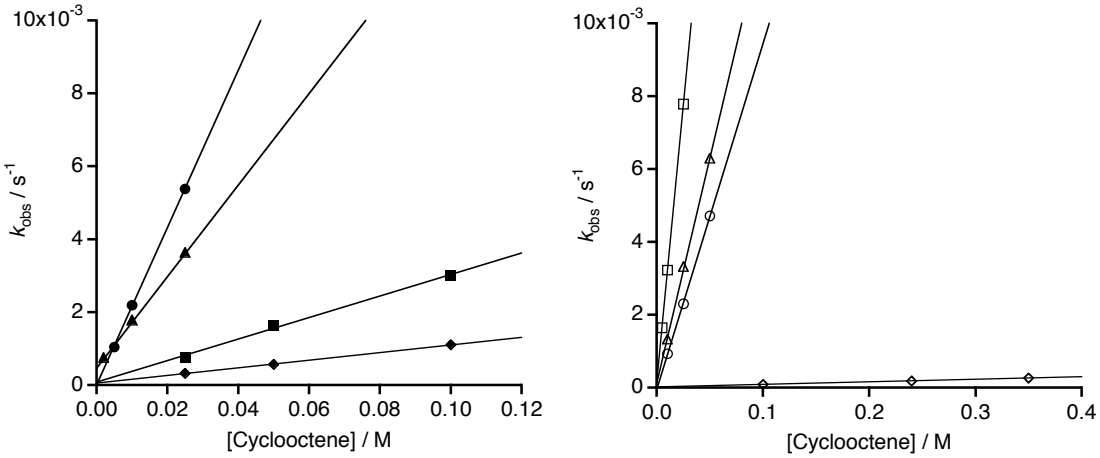

Figure S15. Plot of k_{obs} versus cyclooctene concentration for the reaction of $(TMP^{+\bullet})Fe^{IV}O(L)$ with cyclooctene in dichloromethane at –80°C: $[(TMP^{+\bullet})Fe^{IV}O(Im)](NO_3)$; (●), $(TMP^{+\bullet})Fe^{IV}O(3\text{-F-4-}NO_2\text{-PhO})$; (▲), $[(TMP^{+\bullet})Fe^{IV}O(2\text{-MeIm})](NO_3)$; (■), $(TMP^{+\bullet})Fe^{IV}O(Cl)$; (◆), $[(TMTMP^{+\bullet})Fe^{IV}O(Im)](NO_3)$; (○), $(TMTMP^{+\bullet})Fe^{IV}O(3\text{-F-4-}NO_2\text{-PhO})$; (△), $[(TMTMP^{+\bullet})Fe^{IV}O(2\text{-MeIm})](NO_3)$; (□), $(TMTMP^{+\bullet})\ Fe^{IV}O(NO_3)$; (◇).

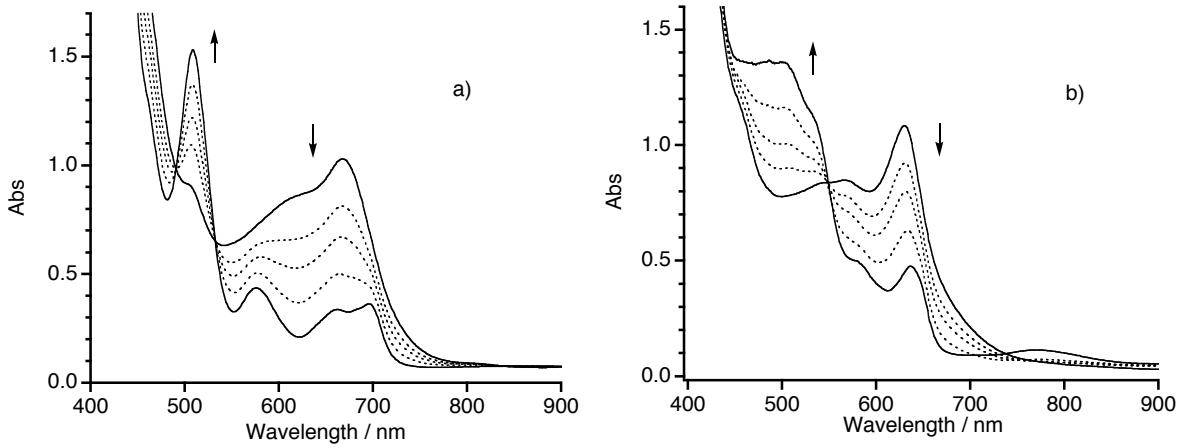

Figure S16. UV-vis absorption spectral change upon addtion of cyclooctene in dichloromethane solution (concentration 100 μM, 1cm path length cell) of $(Por^{+\bullet})Fe^{IV}O(L)$ at –80°C: a) $(TMP^{+\bullet})Fe^{IV}O(Cl)$; b) $(TMTMP^{+\bullet})Fe^{IV}O(NO_3)$.

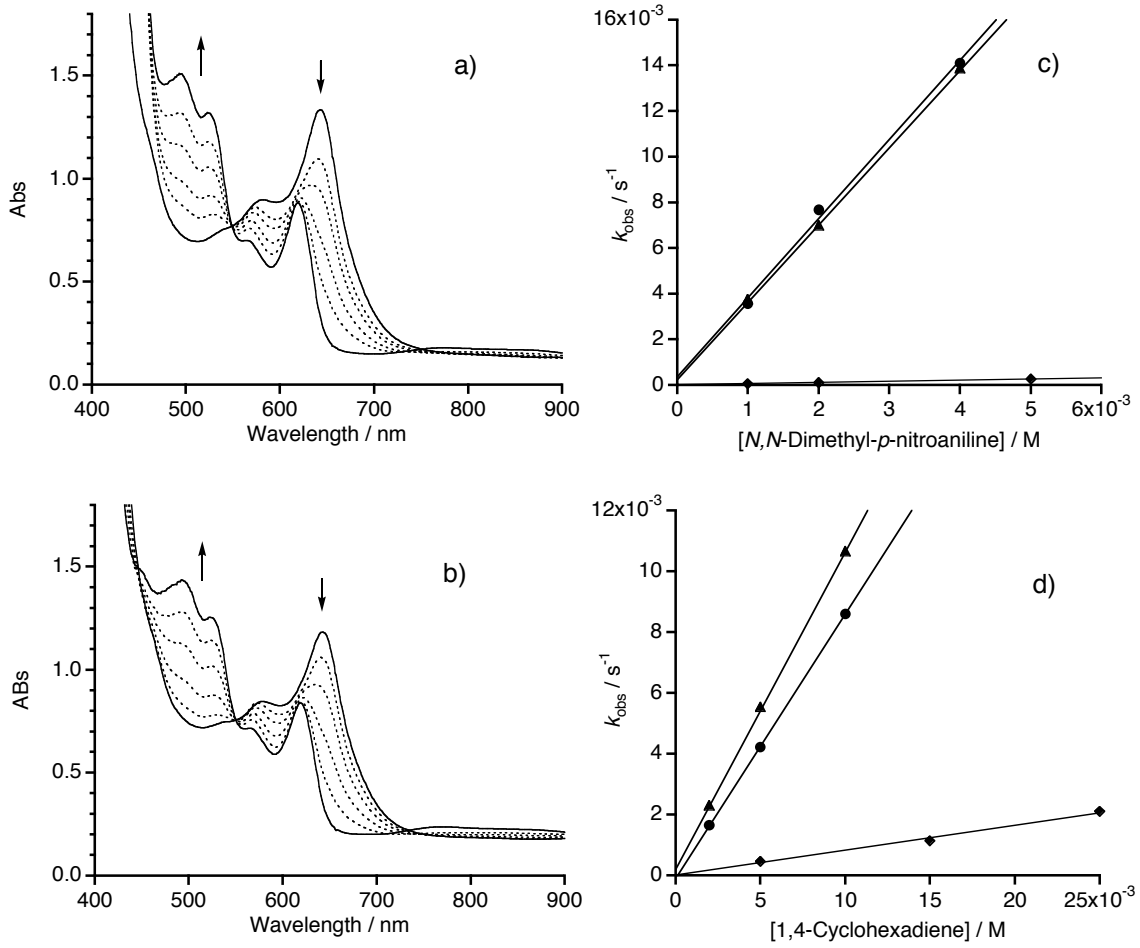

Figure S17. UV-vis Absorption spectral change for the reaction of $(TMTMP^{+\bullet})Fe^{IV}O(3\text{-F-4-}NO_2\text{-PhO})$ with a) *N,N*-dimethyl-*p*-nitroaniline and b) 1,4-cyclohexadiene in dichloromethane solution (concentration 100 μM, 1cm path length cell) at –80°C. Plot of k_{obs} versus substrate concentration for the reaction of $(TMTMP^{+\bullet})Fe^{IV}O(L)$ with c) *N,N*-dimethyl-*p*-nitroaniline and d) 1,4-cyclohexadiene in dichloromethane at –80°C: $[(TMTMP^{+\bullet})Fe^{IV}O(Im)](NO_3)$; (●), $(TMTMP^{+\bullet})Fe^{IV}O(3\text{-F-4-}NO_2\text{-PhO})$; (▲), $(TMP^{+\bullet})Fe^{IV}O(NO_3)$; (◆).

Table S1. The Parent Peak Values (*m/z*) of $[(P^{+\bullet})Fe^{IV}O(L)](ClO_4)$ Determined by ESI-TOF-MS

Porphyrin	L =	Observed	Calculated
TMP	None	852.36 [a]	852.35
	Im	920.44 [a]	920.38
	2-MeIm	934.36 [a]	934.40
	5-MeIm	934.49 [a]	934.40
TMTMP	None	908.11 [b]	908.12
	Im	976.06 [b]	976.45
	2-MeIm	990.96 [b]	990.46
	5-MeIm	990.19 [b]	990.46

[a] In acetnitrile solution at low temperature. [b] In dichloromethane solution at low temperature.

Table S2. ^{1}H NMR Chemical shift (ppm) of $(P)Fe^{IV}=O(L)$ in CD_2Cl_2 at –80°C

Complex	Py-H (Me)	meso-H	*ortho*	*meta*	*para*
$(TMP)Fe^{IV}=O$	6.5		1.0, 3.5	6.0, 6.6	2.7
$(TMP)Fe^{IV}=O$(N-MeIm)	3.8		1.2, 3.8	7.1, 7.2	2.8
$(TMP)Fe^{IV}=O$(1,2-DiMeIm)	4.3		0.9, 3.7	7.0, 7.6	2.7
$(TMTMP)Fe^{IV}=O$	(8.6)	33.3	1.5, 3.8	7.3, 8.8	2.6
$(TMTMP)Fe^{IV}=O$(N-MeIm)	(4.7)	17.2	1.6, 2.8	7.3, 8.1	2.5
$(TMTMP)Fe^{IV}=O$(1,2-DiMeIm)	(4.8)	18.0	1.7, 3.5	7.3, 8.1	2.4